

# Muscle Coactivation in the Sky: Geometry and Pareto Optimality of Energy vs. Promptness in Multirotors

Antonio Franchi<sup>1,2</sup>

**Abstract**—In robotics and human biomechanics, the tension between energy economy and kinematic readiness is well recognized; this work brings that fundamental principle to aerial multirotors. We show that the limited torque of the motors and the nonlinear aerodynamic map from rotor speed to thrust naturally give rise to the novel concept of promptness—a metric akin to dynamic aerodynamic manipulability. By treating energy consumption as a competing objective and introducing a geometric fiber-bundle formulation, we turn redundancy resolution into a principled multi-objective program on affine fibers. The use of the diffeomorphic transformation linearizing the signed-quadratic propulsion model allows us to lay the foundations for a rigorous study of the interplay between these costs. Through an illustrative case study on 4-DoF allocation on the hexarotor, we reveal that this interplay is fiber-dependent and physically shaped by hardware inequalities. For unidirectional thrusters, the feasible fibers are compact, yielding interior allocations and a short Pareto arc, while torque demands break symmetry and separate the optima. Conversely, with reversible propellers, the null space enables antagonistic rotor co-contraction that drives promptness to hardware limits, making optimal endurance and agility fundamentally incompatible in those regimes. Ultimately, rather than relying on heuristic tuning or black box algorithms to empirically improve task execution, this framework provides a foundational understanding of why and how to achieve agility through geometry-aware control allocation, offering possible guidance for vehicle design, certification metrics, and threat-aware flight operation.

## I. INTRODUCTION

Multirotor aerial vehicles with actuation redundancy including standard hexarotors and octocopters, fully actuated hepta- and octocopters [1, 2], and platforms equipped with servomotors [3, 4] possess a nontrivial null space in their control allocation matrix. This redundancy implies a continuous manifold of admissible actuator commands for any given hovering or trajectory-tracking task. Standard allocation schemes typically resolve this freedom by minimizing a proxy for power consumption (often a norm of the motor commands related to rotor speed), using least-norm pseudo-inverse or optimization-based allocators developed in control-allocation theory and widely adopted in aerial platforms.

The ability of a multirotor to reject aggressive disturbances [5] (e.g., wind gusts, aerodynamic ground effects, or payload shifts) or perform agile flight maneuvers [6, 7], depends critically on its *promptness*: the capacity to produce rapid changes in the net wrench under physical limits on rotor acceleration, a notion closely related to manipulability

<sup>1</sup> Robotics and Mechatronics department, Faculty of Electrical Engineering, Mathematics & Computer Science, University of Twente, Enschede, The Netherlands. schol@r-franchi.eu

<sup>2</sup> Department of Computer, Automation and Management, Sapienza University of Rome, Rome, Italy.

in robotics [8]. If a minimal-energy allocation selects an operating point with low promptness, or one close to singular configurations where control authority is diminished along specific directions, the actuators may reach torque or acceleration limits before the required stabilizing wrench can be generated, risking degraded performances or loss of control.

The main thesis of this work is that, in the design and control of multirotor aerial platforms, there exists a fundamental yet poorly understood interplay between operational efficiency (energy saving) and dynamic capability (promptness). The interplay between energy budgeting, promptness (time-critical performance), and physical energy storage/release has been widely explored in robotics—from energy-tank protocols that regulate injected/dissipated work for post-impact safety to compliant-actuation designs that harness elastic storage and field-weakening for peak performance under actuation limits—see, e.g., [9, 10]. While it is well recognized in robotics and biomechanics that biological systems trade metabolic cost for kinematic readiness (e.g., via coactivation or pre-tensioning) [11, 12, 13, 14], this principle has not been formally characterized for aerial robots. Here we present a formal geometric analysis of this conflict in the aerial robotics context. We show that the trade-off between flight endurance and disturbance rejection/agility is not merely heuristic but rooted in the structure of actuator constraints.

**Control Allocation and Energy Minimization:** Standard allocation strategies—both in academic literature and in widely used flight stacks—typically resolve redundancy via Moore–Penrose pseudo-inverses or quadratic programming (QP), with the objective of minimizing a proxy of control effort. Foundational control-allocation works and more recent multi-rotor research formalize these least-norm/optimization paradigms and their handling of actuator bound [2, 3, 4, 15, 16]. Contemporary autopilot implementations instantiate these principles through an effectiveness matrix and least-squares/QP backends [17, 18], emphasizing effort minimization and failure handling, but without explicitly optimizing dynamic readiness of the wrench response. While effective for endurance, such allocators may bias the system toward energetically “lazy” equilibria that can be kinematically sluggish near singular or weak-effectiveness regimes.

**Manipulability in Aerial Robotics:** The concept of manipulability, originally formalized by Yoshikawa for serial manipulators [8], has seen targeted use in aerial robotics, typically in two contexts. In aerial manipulation, manipulability is used to analyze or optimize the arm-end effector dexterity on a flying base, often treating the multirotor primarily as a carrier [19]. In design optimization, manipulability-inspired indices are

employed to guide static actuator geometry (e.g., tilt angles and rotor arrangements) during design [20, 21], rather than as online control objectives. To the best of our knowledge, dynamic manipulability has not been directly applied to the actuator state space of the vehicle itself (i.e., rotor-speed configuration) as a real-time criterion for redundancy resolution.

*Contributions:* The ideas introduced in this work bridge biomechanics and aerial flight control by formalizing actuator co-contraction for multirotors and by characterizing its geometric implications. Our specific contributions are:

- 1) *Domain shift:* We reinterpret manipulability as a dynamic property of instantaneous rotor-speed states, not of an attached limb or fixed geometry. We name this reinterpretation *promptness*: the log-determinant of the Gram matrix of the Jacobian of the velocity-to-wrench map. We show that operating rotors antagonistically at higher speeds plays the same role as joint stiffening in limb control, enlarging the available wrench-acceleration volume.
- 2) *Task-dependent Promptness-Energy Interplay:* We provide, through illustrative case studies, a rigorous characterization of the conflict between consumed power (modeled via an  $L_{1.5}$ -type norm) and promptness as a topological feature of the fiber bundle induced by the actuation map.
- 3) *Role of Actuator Constraints:* we show that depending on the feasible sets, these objectives can range from being compatible to fundamentally conflicting. Hence, standard allocators may implicitly favor endurance over promptness, possibly at the expense of safety in highly disturbed conditions.

## II. ENERGY AND PROMPTNESS IN MULTIROTORS

The core contribution of this section is demonstrating that the *nonlinear* mapping from propeller speed to generated force, coupled with the physical *rate limits* on rotor acceleration, naturally gives rise to the concept of optimizing promptness. Without these two ingredients, promptness as an objective would be trivial: it would be physically meaningless under infinite acceleration capabilities, and strictly constant under a purely linear force model. By formally establishing promptness as a dynamic, state-dependent variable, we unlock the ability to rigorously evaluate its trade-off against energy consumption within a multi-objective optimization framework.

We intentionally adopt the most standard, universally accepted multirotor actuation models for this analysis. This deliberate simplicity serves a specific purpose: to demonstrate that the dichotomy between energy and promptness is not a fragile artifact of complex aerodynamic assumptions or second-order effects. Rather, it is a fundamental, first-order characteristic that emerges directly from the basic physics of multirotor flight.

We recall here only the concepts needed to define the problem, see, e.g., [22] for a complete introduction. Let the state of the propulsion system be defined by the vector of propeller rotational speeds  $v \in \mathbb{R}^n$ , where  $v_i$  represents the angular speed of the brushless motor driving the  $i$ -th rotor. The intensities of the thrust and drag moment produced by

a fixed-pitch propeller are widely modeled as proportional to the signed square of the rotational speed:

$$F_i = k_f v_i |v_i|, \quad M_i = k_m v_i |v_i| \quad (1)$$

where  $k_f$  and  $k_m$  are aerodynamic lift and drag coefficients, respectively [2, 23]. Let  $u_i = v_i |v_i|$  represent the generalized thrust effort. The nonlinear mapping from rotor speeds to the total body wrench coordinates  $w \in \mathbb{R}^6$  (forces and moments) acting on the vehicle's center of mass is a linear combination of individual rotor contributions:

$$w = f(v) = Au = \sum_{i=1}^n \mathbf{a}_i v_i |v_i|, \quad (2)$$

where  $\mathbf{a}_i \in \mathbb{R}^6$  is the  $i$ -th column of the matrix  $A$  encoding the force and moment generated on the body by the  $i$ -th rotor for a unitary input  $u_i = 1$ , and is determined by the design geometry (positions and orientation of the rotor on the chassis).

*Energy (Power Consumption):* Given the speeds at which propellers are operated and the low inertia of blades used in multirotors, the electrical power during flight is dominated by the dissipation generated by aerodynamic drag on the blades. Since the aerodynamic drag torque satisfies  $\tau_{d,i} \propto v_i^2$ , one has  $P_{\text{mech},i} = \tau_{d,i} v_i \propto v_i^3$ , leading to the total power cost modeled as a weighted  $L_3$  norm of actuator speeds:

$$J_1(v) = \sum_{i=1}^n c_i |v_i|^3, \quad (3)$$

with  $c_i$  aggregating aerodynamic/motor constants [23].

*Promptness:* The promptness of the platform—its ability to change the wrench  $w$  instantaneously—is limited by the acceleration capabilities of the motors [22]. The rate of change of the wrench is given by the chain rule:

$$\dot{w} = \frac{\partial f}{\partial v} \dot{v} = J_f(v) \dot{v} \quad (4)$$

where  $J_f(v) = 2A \cdot \text{diag}(|v|)$  is the state-dependent Jacobian (the derivative of  $v_i |v_i|$  is  $2|v_i|$  for  $v_i \neq 0$ , with continuous extension at  $v_i = 0$ ). The rotor acceleration  $\dot{v}$  is physically constrained by the maximum electromagnetic torque of the motor and the rotational inertia of the propeller [22]. Assuming a simplified symmetric bound  $\|\dot{v}\| \leq 1$  (normalized), the set of achievable wrench rates forms a hyper-ellipsoid in the task space (dynamic manipulability ellipsoid). The volume of this ellipsoid is proportional to  $\sqrt{\det(J_f(v) J_f(v)^T)}$ . To optimize promptness, we define as objective the negative log-determinant:

$$J_2(v) = -\frac{1}{2} \ln \det(J_f(v) J_f(v)^T). \quad (5)$$

Since  $\det(J_f J_f^T) = \prod_{i=1}^6 \sigma_i^2(J_f)$ , where  $\sigma_i$  denotes a singular value of  $J_f$ , one has  $J_2(v) = -\sum_{i=1}^6 \ln \sigma_i(J_f)$ , i.e., a spectral barrier that penalizes any singular value approaching zero; using the log turns the product into a sum and yields a convex objective (because  $-\log \det(\cdot)$  is convex on  $\mathbb{S}_{++}$ ), which improves numerical conditioning and is standard in interior-point methods [24]. Minimizing  $J_2$  ensures the allocation stays well-conditioned and maximally prompt, so that

available motor torque is effectively translated into control authority along all six degrees of freedom.

### III. MOTIVATING EXAMPLE: THE DUAL-ACTUATOR

Let us analyze the simplest redundant system: two actuators controlling a single task variable. This low-dimensional example makes the geometry of the conflict explicit. Consider two actuators  $v_1, v_2$  producing a scalar output  $w$  through

$$f(v) := a_1 v_1 |v_1| + a_2 v_2 |v_2| = w, \quad (6)$$

with  $a_1, a_2 > 0$  fixed gains. In this special setting, the energy and promptness objectives defined before become:

- Energy ( $J_1$ ):  $J_1(v) = \sum_{i=1}^2 c_i |v_i|^3$  with  $c_i > 0$ .
- Inverse promptness ( $J_2$ ):  $J_2(v) = -\ln \|\nabla f(v)\|$ . Since  $\nabla f(v) = [2a_1 |v_1|, 2a_2 |v_2|]$ , one gets

$$J_2(v) = -\ln 2 - \frac{1}{2} \ln(a_1^2 v_1^2 + a_2^2 v_2^2). \quad (7)$$

Minimizing  $J_2$  is therefore equivalent (up to an additive constant) to maximizing  $a_1^2 v_1^2 + a_2^2 v_2^2$ , pushing the state away from the origin, where the gradient of  $f$  vanishes.

*Geometry of the Constraint (The Fiber):* The feasible set  $\mathcal{F}_w := \{v \in \mathbb{R}^2 \mid f(v) = w\}$  is a union of conic arcs in the  $(v_1, v_2)$ -plane whose type depends on the quadrant (i.e., on the signs of  $v_1, v_2$ ) and on  $\text{sgn}(w)$ :

- 1) Cooperative mode (bounded ellipses). This occurs when the actuators align with the task:  $\text{sgn}(v_1) = \text{sgn}(v_2) = \text{sgn}(w)$ .
  - If  $w > 0$  and  $v$  lies in Quadrant I  $(+, +)$ , then  $a_1 v_1^2 + a_2 v_2^2 = w$ .
  - If  $w < 0$  and  $v$  lies in Quadrant III  $(-, -)$ , then  $-a_1 v_1^2 - a_2 v_2^2 = w$ , i.e.,  $a_1 v_1^2 + a_2 v_2^2 = |w|$ .

In both cases the fiber within the quadrant is an elliptical arc (bounded). Along these arcs,  $|v_i|$  is bounded, hence  $J_1$  is bounded from above at fixed  $w$ .

- 2) Antagonistic mode (unbounded hyperbolas). This occurs in the mixed-sign quadrants where actuators oppose each other. Independently of the sign of  $w$ , one gets indefinite quadrics:

- Quadrant II ( $v_1 < 0, v_2 > 0$ ):  $-a_1 v_1^2 + a_2 v_2^2 = w$ .
- Quadrant IV ( $v_1 > 0, v_2 < 0$ ):  $a_1 v_1^2 - a_2 v_2^2 = w$ .

These branches extend to infinity: one can keep  $w$  constant while increasing  $|v_1|$  and  $|v_2|$  simultaneously (internal loading), thereby increasing  $a_1^2 v_1^2 + a_2^2 v_2^2$  (improving promptness) at the cost of larger  $J_1$ .

The geometry of fibers, the energy/promptness fields, and the cost profiles in cooperative vs antagonistic regimes are summarized in Fig. 1

#### A. Conflict Analysis in Effort Coordinates

To analyze the conflict, it is convenient to switch to the coordinates  $u_i := v_i |v_i|$ . In these variables the constraint becomes linear:

$$a_1 u_1 + a_2 u_2 = w, \quad (8)$$

i.e., a straight line in the  $(u_1, u_2)$ -plane (see Fig 1f). The curved fibers seen in the velocity domain are the pre-images of this line under  $u_i = v_i |v_i|$ .

Using  $|u_i| = v_i^2$  and  $|v_i| = (|u_i|)^{1/2}$ , the costs read

$$\tilde{J}_1(u) = c_1 |u_1|^{3/2} + c_2 |u_2|^{3/2}, \quad (9)$$

$$\tilde{J}_2(u) = -\ln 2 - \frac{1}{2} \ln(a_1^2 |u_1| + a_2^2 |u_2|). \quad (10)$$

Thus minimizing  $\tilde{J}_2$  is equivalent to maximizing

$$D(u) = a_1^2 |u_1| + a_2^2 |u_2|.$$

We now evaluate the objectives along the constraint line (the fiber) in these coordinates. Without loss of generality let us assume that  $w > 0$  and we focus our attention on the first and second quadrant.

1) *Cooperative Regime* ( $u_1 > 0, u_2 > 0$ ): For  $w > 0$ , the feasible set is the line segment joining  $(w/a_1, 0)$  and  $(0, w/a_2)$ .

- Energy ( $\tilde{J}_1$ ):  $\tilde{J}_1$  is strictly convex on the segment. With a Lagrange multiplier  $\lambda$  for  $a_1 u_1 + a_2 u_2 = w$  and  $u_i > 0$ ,

$$\begin{aligned} \frac{\partial}{\partial u_i} (c_i u_i^{3/2} + \lambda a_i u_i) &= 0 \Rightarrow \\ \frac{3}{2} c_1 \sqrt{u_1} + \lambda a_1 &= 0, \quad \frac{3}{2} c_2 \sqrt{u_2} + \lambda a_2 = 0, \end{aligned} \quad (11)$$

which yields the optimal sharing rule

$$\frac{u_1}{u_2} = \left( \frac{a_1 c_2}{a_2 c_1} \right)^2.$$

identifying the point on the cooperative segment that lies on the line through the origin with slope  $\left( \frac{a_2 c_1}{a_1 c_2} \right)^2$ . In the special case  $c_1 = c_2$  and  $a_1 = a_2$ , this reduces to  $u_1 = u_2$ , i.e., the midpoint of the segment.

- Promptness ( $\tilde{J}_2$ ): Along the segment,  $u_2 = (w - a_1 u_1)/a_2$  and

$$D(u_1) = a_1^2 u_1 + a_2^2 \frac{w - a_1 u_1}{a_2} = a_1 (a_1 - a_2) u_1 + a_2 w,$$

which is linear in  $u_1$ . If  $a_1 = a_2$ ,  $\tilde{J}_2$  is constant (indifferent). If  $a_1 \neq a_2$ ,  $\tilde{J}_2$  is monotone and prefers the corner that uses only the actuator with larger  $a_i$ .

*Conclusion:* Minimal conflict.  $\tilde{J}_2$  is indifferent or weakly biased to a corner, whereas  $\tilde{J}_1$  has a strong convex basin that favors an interior load distribution. An energy-only based allocation distributes the load and does not drive promptness too far from its optimum in this region.

- 2) *Antagonistic Regime* ( $u_1 < 0, u_2 > 0$ ): Here the feasible set is an unbounded ray. From  $a_1 u_1 + a_2 u_2 = w$  one gets

$$|u_2| = \frac{w}{a_2} + \frac{a_1}{a_2} |u_1|.$$

- Energy ( $\tilde{J}_1$ ): Since  $|u_2|$  grows linearly with  $|u_1|$ , the sum  $c_1 |u_1|^{3/2} + c_2 |u_2|^{3/2}$  increases strictly with distance from the origin, pushing toward the boundary  $u_1 \rightarrow 0$  (minimum viable effort).

- Promptness ( $\tilde{J}_2$ ): Substituting the ray relation into  $D$  gives

$$D = a_1^2 |u_1| + a_2^2 \left( \frac{w}{a_2} + \frac{a_1}{a_2} |u_1| \right) = (a_1^2 + a_1 a_2) |u_1| + a_2 w,$$

with strictly positive slope. Along the ray, promptness improves without bound as  $|u_1| \rightarrow \infty$  (so  $\tilde{J}_2 \rightarrow -\infty$ ).

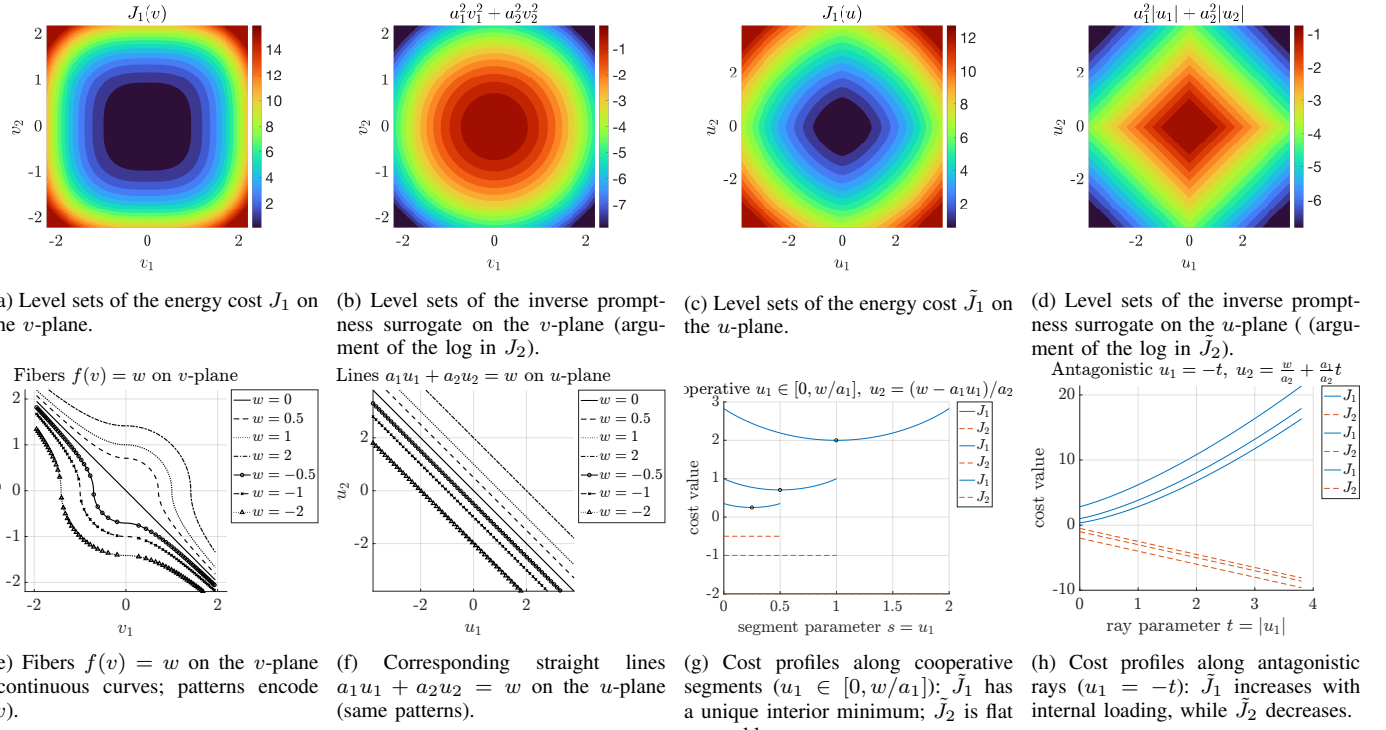


Fig. 1: Dual-actuator case study summary. (a)–(d) show energy cost and inverse promptness fields on the rotor speed ( $v$ ) and control effort ( $u$ ) planes. (e) Continuous elliptic/hyperbolic fibers on the  $v$ -plane for several  $w$  values, visually differentiated by seven distinct line patterns. (f) The same family maps to straight lines on the  $u$ -plane with consistent patterns. (g) On cooperative segments, the energy  $\tilde{J}_1$  attains a strict interior minimum while  $\tilde{J}_2$  is indifferent or only weakly biased, indicating minimal conflict. (h) On antagonistic rays,  $\tilde{J}_1$  and  $\tilde{J}_2$  exhibit opposing trends, illustrating total conflict under internal loading.

**Conclusion:** Total conflict. Energy optimization pulls to the lazy boundary (zero internal force), whereas promptness optimization drives toward unbounded internal loading (maximum co-contraction/coactivation).

3) **Summary:** This case study reveals some fundamental facts linking the task-fiber geometry and actuator limits to the interplay between the two optimization objectives:

- Some actuation regions may slice fibers of  $f$  which are roughly aligned with the level curves of the two objectives and yield compatibility and load distribution.
- Some other actuation regions may slice fibers  $f$  which are roughly aligned with the opposing gradients of the two objectives and induce a fundamental dichotomy between energy and promptness.

#### IV. GENERAL FRAMEWORK: MOO ON FIBERS

We now place the specific dual-objective problem (energy vs. promptness) into a general geometric setting for multi-objective optimization (MOO) on redundant robotic systems. The goal is to formalize (i) where redundancy lives, (ii) how objectives interact when restricted to a redundancy manifold, and (iii) how physical inequalities reshape this interaction. This formalization provides a general reference and mindset for the illustrative study of section V and future works on the topic.

Let  $\mathcal{E}$  be the  $n$ -dimensional total space (the manifold of actuator configurations) and  $\mathcal{B}$  be the  $m$ -dimensional base

space (the manifold of task outputs), with  $m < n$ . We assume a smooth, surjective submersion  $\pi : \mathcal{E} \rightarrow \mathcal{B}$ , which maps an internal configuration  $v \in \mathcal{E}$  (e.g., rotor speeds) to a task value  $w \in \mathcal{B}$  (e.g., wrench). The submersion hypothesis implies that the Jacobian  $J_\pi(v) \in \mathbb{R}^{m \times n}$  has full row rank  $m$  for all  $v$  in the region of interest.

**Definition 1** (Fiber). Given  $w \in \mathcal{B}$ , the *fiber* associated with  $w$  is the level set

$$\mathcal{F}_w := \pi^{-1}(w) = \{v \in \mathcal{E} \mid \pi(v) = w\}. \quad (12)$$

Since  $\pi$  is a submersion, the implicit function theorem guarantees that  $\mathcal{F}_w$  is a smooth submanifold of  $\mathcal{E}$  of dimension  $k = n - m$ .

**Definition 2** (Tangent space and orthogonal projector). For any  $v \in \mathcal{F}_w$ , the tangent space to the fiber is

$$T_v \mathcal{F}_w = \ker(d\pi_v) = \ker(J_\pi(v)), \quad (13)$$

where  $\ker(J_\pi(v)) = \{\delta v \in \mathbb{R}^n \mid J_\pi(v) \delta v = 0\}$ . With the standard Euclidean inner product on  $\mathbb{R}^n$ , the orthogonal projector onto  $T_v \mathcal{F}_w$  is

$$P_v = I_n - J_\pi(v)^\top \left( J_\pi(v) J_\pi(v)^\top \right)^{-1} J_\pi(v), \quad (14)$$

which is well-defined under the full-row-rank assumption on  $J_\pi(v)$ .

Let  $J_1, J_2 : \mathcal{E} \rightarrow \mathbb{R}$  be smooth objectives. In our application,  $J_1$  models energetic cost (e.g., weighted  $\ell_3$  norm of speeds) and  $J_2$  models promptness/readiness (e.g., negative log-determinant of the Gramian of  $J_\pi$  or a monotone surrogate), but here we keep them abstract.

**Definition 3** (Restricted gradient on the fiber). The gradient of  $J_i$  restricted to  $\mathcal{F}_w$  is

$$\nabla_{\mathcal{F}_w} J_i(v) := P_v \nabla J_i(v) \in T_v \mathcal{F}_w. \quad (15)$$

When  $\nabla_{\mathcal{F}_w} J_i(v) = 0$ , we call  $v$  a *fiber-stationary* point for  $J_i$ .

**Definition 4** (Local alignment (conflict) index). Let  $v \in \mathcal{F}_w$  with  $\nabla_{\mathcal{F}_w} J_1(v)$  and  $\nabla_{\mathcal{F}_w} J_2(v)$  not both zero. Define

$$\kappa(v) = \frac{\langle -\nabla_{\mathcal{F}_w} J_1(v), -\nabla_{\mathcal{F}_w} J_2(v) \rangle}{\|\nabla_{\mathcal{F}_w} J_1(v)\| \|\nabla_{\mathcal{F}_w} J_2(v)\|} \in [-1, 1]. \quad (16)$$

Then:

- $\kappa(v) = 1$ : the restricted gradients are aligned (local *compatibility*).
- $\kappa(v) = -1$ : the restricted gradients are anti-aligned (local *conflict*).
- $\kappa(v) = 0$ : the restricted gradients are orthogonal (local *independence*).

If one restricted gradient vanishes,  $\kappa$  is undefined; by convention we may set  $\kappa(v) = 1$  when *both* vanish (a shared fiber-stationary point), and treat the single-objective stationary case separately.

**Definition 5** (Local Pareto optimality on the fiber). A point  $v^* \in \mathcal{F}_w$  is a (first-order) local Pareto optimum if there is no nonzero  $\delta v \in T_{v^*} \mathcal{F}_w$  such that both directional derivatives are negative:

$$\langle \nabla_{\mathcal{F}_w} J_1(v^*), \delta v \rangle < 0 \quad \text{and} \quad \langle \nabla_{\mathcal{F}_w} J_2(v^*), \delta v \rangle < 0.$$

Equivalently, there exist  $\lambda_1, \lambda_2 \geq 0$ , not both zero, such that

$$\lambda_1 \nabla_{\mathcal{F}_w} J_1(v^*) + \lambda_2 \nabla_{\mathcal{F}_w} J_2(v^*) = 0. \quad (17)$$

If both restricted gradients are nonzero, this is the collinearity/anti-parallelism condition ( $\kappa(v^*) = -1$ ). If one restricted gradient vanishes at  $v^*$ , the other must also vanish for Pareto optimality.

*Feasibility and hardware inequalities:* Real actuators obey inequality constraints (e.g., non-negativity, saturation limits, rate limits). Let  $\mathcal{A} \subset \mathcal{E}$  be the admissible region. The relevant domain is then the *feasible fiber*

$$\tilde{\mathcal{F}}_w := \mathcal{F}_w \cap \mathcal{A}. \quad (18)$$

Interior points of  $\tilde{\mathcal{F}}_w$  obey the tangent-space conditions above. At boundary points, the tangent space must be replaced by the tangent cone of  $\tilde{\mathcal{F}}_w$ , and  $P_v$  by the projector onto that cone; correspondingly, Pareto conditions are formulated with feasible directions in the cone.

**Definition 6** (Pareto set and a global conflict measure). Let  $\mathcal{P}_w \subset \tilde{\mathcal{F}}_w$  be the set of local Pareto optima on the feasible

fiber. The image  $\mathbf{J}(\mathcal{P}_w) = \{(J_1(v), J_2(v)) : v \in \mathcal{P}_w\} \subset \mathbb{R}^2$  is the Pareto front in cost space. A simple global conflict index is the *Pareto extent*, defined as the arc length of  $\mathbf{J}(\mathcal{P}_w)$ :

- Zero extent: a single point (near total compatibility).
- Large (possibly unbounded) extent: severe trade-off spanning a wide range of costs (strong conflict).

*Fiber dependence of the interplay:* The interaction between objectives is critically *fiber-dependent*. As the task  $w$  moves in  $\mathcal{B}$ , or as the feasibility region  $\mathcal{A}$  slices different partitions of the full fiber  $\mathcal{F}_w$ , the topology and geometry of the feasible fiber  $\tilde{\mathcal{F}}_w$  can change dramatically (e.g., from compact to non-compact). This shift can completely alter the interplay between the objectives. For instance, consider the constraint  $x|x| + y|y| = w$  with  $w > 0$ . If the feasibility region restricts the system to  $x, y > 0$ , the feasible fiber  $\tilde{\mathcal{F}}_w$  is a compact circular arc ( $x^2 + y^2 = w$ ), where continuous objectives naturally attain finite minima. In contrast, if the feasibility region restricts the system to  $x < 0, y > 0$ ,  $\tilde{\mathcal{F}}_w$  becomes a non-compact hyperbolic branch ( $-x^2 + y^2 = w$ ). The geometry and direction of the fiber are fundamentally transformed compared to the previous case. This topological shift reshapes the restricted gradients, and antagonistic costs may now drive solutions toward infinity along distinct branches, creating an entirely different conflict regime. Thus, whether two costs are “friends” or “enemies” is not an absolute property of the costs themselves, but depends entirely on the specific *feasible fiber*  $\tilde{\mathcal{F}}_w$  they are currently restricted to.

#### A. Fundamental Research Questions

This geometric view of redundancy resolution motivates three guiding questions:

- 1) **Compatibility along a fiber.** For a given task  $w$ , how do the objectives interact on the feasible fiber  $\tilde{\mathcal{F}}_w$ ? Do they share a unique minimizer (indicating high compatibility), or are they anti-aligned (indicating conflict)? How severe is the conflict (e.g., as measured by the Pareto extent)?
- 2) **Topological dependence across tasks.** Does the interplay remain qualitatively the same throughout  $\mathcal{B}$ , or do changes in  $\mathcal{F}_w$  (e.g., transitions between compact and non-compact fibers, or changes in conditioning) induce regime switches between compatible and conflicting behaviors?
- 3) **Impact of hardware constraints.** How does the admissible region  $\mathcal{A}$  reshape  $\tilde{\mathcal{F}}_w$  and the associated Pareto set? Do inequality constraints neutralize, create, or amplify conflicts that would otherwise not exist on the unconstrained fiber?

This abstract framework is not specific to aerial robotics and multirotors: it applies to any redundant system (e.g., soft robots, human biomechanics, multi-limb manipulation). Hopefully, this formalization will prove useful to a broader scientific community.

## V. PROMPTNESS VS. ENERGY IN HEXAROTOR 4-DOF WRENCH ALLOCATION

Rather than pursuing an exhaustive theoretical treatise, our objective in this section is to ground the proposed geometric

framework in a ubiquitous and highly relevant robotic application. By examining a concrete case study, we aim to uncover a rich, diverse set of practical insights that illustrate the complex geometry of redundancy resolution. This approach not only validates our methodology but also establishes a robust foundation for extending these findings to other multi-actuated, redundant platforms in future work.

To this end, we instantiate our fiber-based analysis on a standard coplanar hexarotor—a widely used platform whose six propellers generate thrust collinear with the body’s  $+z$ -axis.

The vehicle is underactuated in full 6-DoF, but *redundant* for the standard 4-DoF wrench task

$$w = [\tau_x \ \tau_y \ \tau_z \ F_z]^\top \in \mathbb{R}^4,$$

with allocation map  $A \in \mathbb{R}^{4 \times 6}$  built from the arm position coordinates  $r_i = [x_i, y_i, 0]^\top$  and spin directions  $\sigma_i \in \{\pm 1\}$ :

$$A = \begin{bmatrix} k_f y_1 & \dots & k_f y_6 \\ -k_f x_1 & \dots & -k_f x_6 \\ k_m \sigma_1 & \dots & k_m \sigma_6 \\ k_f & \dots & k_f \end{bmatrix}, \quad w = Au. \quad (19)$$

with  $u_i := v_i |v_i|$ . For typical symmetric layouts,  $A$  has full row rank 4; hence, for any feasible  $w$ , the fiber in the  $u$ -space

$$\mathcal{F}_w^u = \{u \in \mathbb{R}^6 \mid Au = w\}$$

is a 2-dimensional affine plane. On this fiber, we compare the  $u$ -space rewritten energy objective and promptness surrogate:

$$\tilde{J}_1(u) = \sum_{i=1}^6 c_i |u_i|^{3/2}, \quad \tilde{J}_2(u) = -\frac{1}{2} \log \det(S(u)),$$

with  $S(u) = A \Sigma(u) A^\top$ , and  $\Sigma(u) = \text{diag}(|u|)$ . This  $\tilde{J}_2$  is equivalent (up to an additive constant) to the negative log-determinant of the dynamic manipulability Gramian in the  $v$ -coordinates, since  $J_f(v) = 2A \text{diag}(|v|)$  and  $|v| = \sqrt{|u|}$  imply  $J_f(v) J_f(v)^\top = 4A \text{diag}(|u|) A^\top = 4S(u)$ .

#### A. Unidirectional speeds: $u \geq 0$ (standard ESCs)

The feasible fiber at a given  $w$  is the convex polygon

$$\tilde{\mathcal{F}}_w^u = \mathcal{P}_w := \{u \in \mathbb{R}_{\geq 0}^6 \mid Au = w\}, \quad (20)$$

which is nonempty precisely when  $w$  belongs to the wrench cone generated by the columns of  $A$ . On  $\mathcal{P}_w$ :

- *Energy optimum.* Since  $p = \frac{3}{2} > 1$ ,  $\tilde{J}_1$  is strictly convex. Thus  $\min_{u \in \mathcal{P}_w} \tilde{J}_1(u)$  admits a unique solution  $u_{\text{en}}^*$ , which is typically interior when the geometry is nondegenerate. The KKT stationarity for active indices ( $u_i > 0$ ) reads

$$\frac{3}{2} c_i \sqrt{u_i} = \lambda^\top a_i, \quad (21)$$

equalizing the marginal energetic costs across the active rotors, where  $a_i$  denotes the  $i$ -th column of  $A$  and  $\lambda \in \mathbb{R}^4$  is the multiplier for the wrench constraint  $Au = w$ .

- *Promptness optimum.* Since  $S(u) = \sum_{i=1}^6 u_i a_i a_i^\top$  is linear in  $u$  over  $\mathbb{R}_{\geq 0}^6$  and  $\log \det(\cdot)$  is strictly concave on  $\mathbb{S}_{++}$

[24], the composition  $u \mapsto \log \det S(u)$  is strictly concave for all  $u$  with  $S(u) \succ 0$ . Hence

$$\max_{u \in \mathcal{P}_w} \log \det S(u)$$

has a unique maximizer  $u_{\text{pr}}^*$  whenever the active columns at the optimum span  $\mathbb{R}^4$ . Its stationarity for active indices is

$$a_i^\top S(u)^{-1} a_i = \eta^\top a_i \quad (u_i > 0), \quad (22)$$

which equalizes the marginal promptness gain  $a_i^\top S(u)^{-1} a_i$  against the wrench constraints (with multiplier  $\eta \in \mathbb{R}^4$ ).

*Comparison:* Both  $u_{\text{en}}^*$  and  $u_{\text{pr}}^*$  typically avoid the boundary faces of  $\mathcal{P}_w$ , promoting distributed allocations ( $u_i > 0$  for most  $i$ ). They generally do not coincide, instead, they anchor the endpoints of a Pareto set that forms a compact arc through the interior of  $\mathcal{P}_w$ . In fact, the achievable promptness is strictly finite because  $\mathcal{P}_w$  is bounded. This is because unidirectionality ( $u_i \geq 0$ ) and the thrust row in (19) enforce  $F_z = k_f \sum_{i=1}^6 u_i \Rightarrow 0 \leq u_i \leq \frac{F_z}{k_f}$ , so no null-space direction  $\Delta u \in \ker(A)$  can increase all rotor efforts simultaneously: the equality  $\mathbf{1}^\top \Delta u = 0$  (implied by the thrust row of  $A$ ) forces mixed signs in  $\Delta u$ , and any attempt to “co-contract” inevitably drives some  $u_i$  toward the forbidden negative half-space. Consequently,  $\mathcal{P}_w$  is closed and bounded, which precludes unbounded increases of promptness in the unidirectional regime.

*Wrench-Dependent Objective Conflict:* The divergence between  $u_{\text{en}}^*$  and  $u_{\text{pr}}^*$  is *fiber-dependent*: it is governed by the specific feasible fiber  $\mathcal{P}_w$  induced by the commanded wrench  $w$ . For a perfectly symmetric platform (geometry, spin pattern, and weights  $c_i = c$ ) and a pure-thrust command  $w = [0, 0, 0, F_z]^\top$ , the fiber and both KKT systems are permutation-symmetric. In this case the optima coincide at the isotropic allocation  $u_{\text{en}}^* = u_{\text{pr}}^* = \frac{F_z}{6k_f} \mathbf{1}$  (provided the spin pattern satisfies  $\sum_i \sigma_i = 0$ ), and the Pareto set collapses to a single point.

The coincidence breaks as soon as a nonzero torque is required together with thrust (e.g.,  $w = [0, \tau_y, 0, F_z]^\top$ ), which is typical when compensating an off-center payload or steady aerodynamic drag. From the energy KKT condition (21) (with  $u_i > 0$ ) one obtains  $\sqrt{u_i} \propto \lambda^\top a_i$ , hence

$$u_i \propto (\lambda^\top a_i)^2 = (k_f(\lambda_1 y_i - \lambda_2 x_i + \lambda_4) + k_m \lambda_3 \sigma_i)^2,$$

i.e., a *quadratic* spatial profile in the rotor features  $(x_i, y_i, \sigma_i)$ . In contrast, the promptness KKT stationarity is (22), which equates the (nonlinear) marginal gains  $a_i^\top S^{-1} a_i$  to a *linear* function of the rotor features,  $\eta^\top a_i = k_f(\eta_1 y_i - \eta_2 x_i + \eta_4) + k_m \eta_3 \sigma_i$ . Because generating  $\tau_y \neq 0$  necessarily skews  $S(u)$ , there is, generically, no allocation  $u$  for which the quadratic energy profile and the linear promptness balance can be satisfied simultaneously (except for measure-zero symmetric cases such as  $\tau_y = 0$ ). Therefore the two optima diverge, defining a compact Pareto arc in the interior of the fiber.

### B. Bidirectional speeds with bounds: $|u_i| \leq \bar{u}_i$

Allowing reversible rotor effort expands the feasible set from the simplex-like  $\mathcal{P}_w$  to a centrally symmetric, box-constrained affine slice we obtain different feasible fiber:

$$\tilde{\mathcal{F}}_w^u = \mathcal{Q}_w := \{u \in \mathbb{R}^6 \mid Au = w, |u_i| \leq \bar{u}_i \forall i\}.$$

Dropping nonnegativity removes the simplex cap imposed by the thrust row (i.e.,  $0 \leq u_i \leq \frac{F_z}{k_f}$ ), exposing directions in the null space  $\ker(A)$  with mixed signs. Hence one can superimpose antagonistic internal commands  $\Delta u \in \ker(A)$  onto any baseline feasible allocation without altering  $w$ , until box limits are met. This changes the geometry of the two optimization problems:

- *Energy optimum* ( $u_{\text{en}}^*$ ). The objective  $\tilde{J}_1(u) = \sum_i c_i |u_i|^{3/2}$  is strictly convex on  $\mathbb{R}^6$ , so  $\min_{u \in \mathcal{Q}_w} \tilde{J}_1(u)$  has a unique solution. Antagonistic internal loads (nonzero  $\Delta u \in \ker(A)$ ) generally *increase*  $\tilde{J}_1$ , so the optimizer suppresses “co-contraction” and gravitates toward the minimum-effort feasible point. If the unconstrained minimizer respects the bounds,  $u_{\text{en}}^*$  lies in the interior; otherwise, it touches the smallest necessary set of box faces.
- *Promptness optimum* ( $u_{\text{pr}}^*$ ). With  $S(u) = \sum_i |u_i| a_i a_i^\top$ , the map  $u \mapsto \log \det S(u)$  is strictly concave on  $\{u : S(u) \succ 0\}$  and is *monotone nondecreasing* in each magnitude  $|u_i|$ . Along feasible directions in  $\ker(A)$ , one can increase selected magnitudes  $|u_i|$  to expand  $S(u)$  in the least-excited directions, thereby increasing  $\log \det S(u)$  until halted by the box. Hence the maximizer of  $\max_{u \in \mathcal{Q}_w} \log \det S(u)$  tends to resides on the boundary  $\partial \mathcal{Q}_w$ , possibly saturating one or several actuators:  $|u_i| = \bar{u}_i$ .

### C. Discussion

*Takeaway:* For a standard 4-DoF underactuated hexarotor with a full-row-rank allocation map  $A \in \mathbb{R}^{4 \times 6}$ , the redundancy has dimension  $\dim \ker(A) = 6 - 4 = 2$ . In the unidirectional regime ( $u \geq 0$ ), positivity truncates this null space, confining both optima to a compact feasible polygon and yielding a short, interior Pareto arc. In contrast, in the bidirectional regime ( $|u_i| \leq \bar{u}_i$ ), the promptness formulation deliberately exploits the 2-D null space to induce antagonistic co-contraction. The divergence between efficiency and agility becomes pronounced: the energy optimum remains anchored near the center of the fiber (suppressing internal loads), whereas the promptness optimum is driven along  $\ker(A)$  until arrested by hardware limits, saturating multiple actuators.

*Geometric Origin of the Boundary Divergence:* The reason promptness is bounded in the unidirectional regime but saturates box limits in the bidirectional regime lies in the interaction between the allocation null space  $\ker(A)$  and the nonnegative orthant. The promptness objective  $\log \det(S(u))$  is monotone nondecreasing in each magnitude  $|u_i|$ . To increase these magnitudes without altering  $w$ , the optimizer must move along a null-space direction  $\Delta u \in \ker(A)$ . For coplanar multirotors thrusting along the body  $+z$ , the last row of  $A$  is

strictly positive ( $k_f \mathbf{1}^\top$ ). Hence any  $\Delta u \in \ker(A)$  must satisfy  $\mathbf{1}^\top \Delta u = 0$ , which forces mixed signs. Equivalently,

$$\ker(A) \cap \mathbb{R}_{\geq 0}^6 = \{0\}.$$

Therefore, under unidirectionality ( $u \in \mathbb{R}_{\geq 0}^6$ ), one cannot inject a null-space direction that strictly increases all  $|u_i|$  simultaneously: any feasible traversal along  $\ker(A)$  necessarily drives some coordinates toward the orthant boundary ( $u_i \rightarrow 0$ ). This orthant confinement makes  $\mathcal{P}_w = \{u \geq 0 \mid Au = w\}$  compact and arrests promptness at an interior compromise. Conversely, in the bidirectional regime the state is not confined to a single orthant: mixed-sign  $\Delta u \in \ker(A)$  can increase selected magnitudes  $|u_i|$  while canceling net wrench, so the promptness climbs along  $\ker(A)$  until the box  $|u_i| \leq \bar{u}_i$  is met, pushing the solution to  $\partial \mathcal{Q}_w$ .

*Dimensionality and the Cauchy–Binet Expansion:* For the promptness objective there is a distinction between boundary-seeking behavior in scalar tasks ( $m = 1$ , cf. Sec. III) and the just discussed interior optima in multi-DoF tasks ( $m \geq 2$ ) which is rooted in the determinant’s algebra. For  $m = 1$  one has  $S(u) = \sum_{i=1}^n a_i^2 |u_i|$  (here  $a_i \in \mathbb{R}$ ), so  $\log S(u)$  is strictly monotone along any feasible null-space direction; with no interior critical point, the optimizer slides toward the admissible boundary (e.g., some  $u_i \rightarrow 0$  in the unidirectional case). For  $m \geq 2$ , by Cauchy–Binet,

$$\det(S(u)) = \sum_{\substack{K \subset \{1, \dots, n\} \\ |K|=m}} \det(A_K)^2 \prod_{k \in K} |u_k|,$$

where  $A_K$  collects the columns indexed by  $K$ . Thus  $\det(S(u))$  is a positive linear combination of degree- $m$  cross-terms (e.g.,  $|u_i| |u_j|$  for  $m = 2$ ), and  $\log \det(S(u))$  is strictly concave in  $S$  and concave in  $u$ . Geometrically, maximizing such products under affine wrench constraints favors *balanced* interior allocations, repelling the solution from faces where some  $|u_i| = 0$ . This explains why in the unidirectional regime the promptness optimum  $u_{\text{pr}}^*$  lies in the interior of  $\mathcal{P}_w$  for the hexarotor ( $m = 4$ ) while in the  $m = 1$  case of Sec. III it was in general on the boundary.

### D. Numerical Simulations

Figure 2 illustrates the redundancy resolution outcomes for a coplanar hexarotor with the following configuration: mass  $m = 0.5 \text{ kg}$  (so  $F_z = mg = 4.905 \text{ N}$ ), arm radius  $R = 0.25 \text{ m}$ , gains  $k_f = 1.0$  and  $k_m = 0.05$ , standard  $60^\circ$  layout, and alternating spins. We sweep the roll torque  $\tau_x \in [0, 1.0] \text{ N m}$  with  $\tau_y = \tau_z = 0$ , and compare the energy-optimal allocation (minimizing  $\tilde{J}_1 = \sum c_i |u_i|^{3/2}$  with  $c_i = 1$ ) against the promptness-optimal allocation (maximizing  $\log \det S$  via minimizing  $\tilde{J}_2 = -\frac{1}{2} \log \det S$  with  $S(u) = A \text{diag}(|u|) A^\top$ ). Because the promptness objective is non-convex particularly in the bidirectional regime where rotor speeds can cross zero, the optimization is performed using an interior-point algorithm augmented with a multi-seed initialization strategy across the allocation null space, followed by strict pruning.

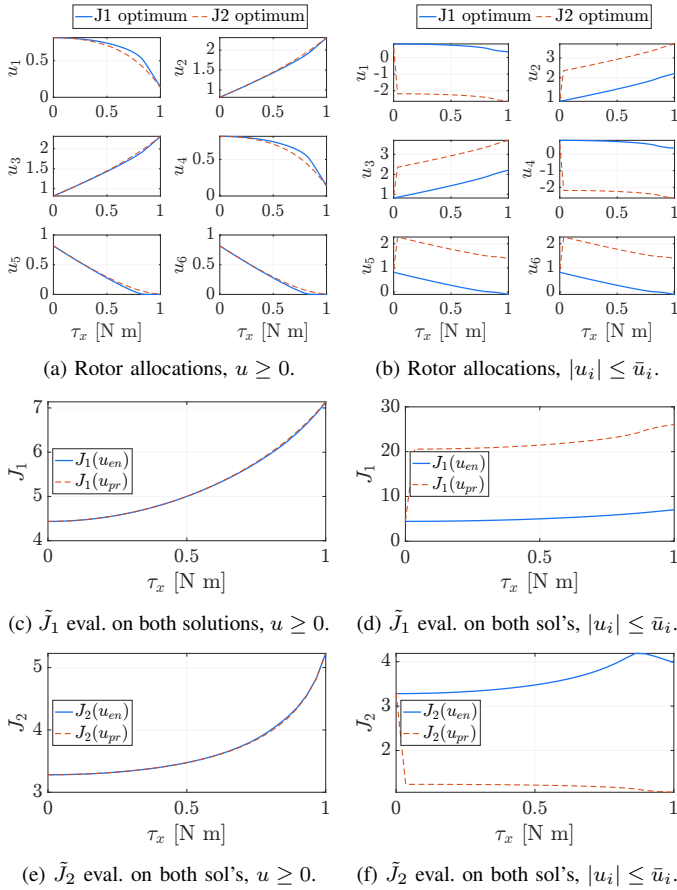


Fig. 2: Hexarotor redundancy resolution under a roll-torque sweep: two actuation regimes are shown: *unidirectional* ( $u \geq 0$ ; left column) and *bidirectional with box bounds* (right column) with  $|u_i| \leq \bar{u}_i$  and  $\bar{u}_i = 5$ . In each regime we overlay the energy-optimal allocation and the promptness-optimal allocation, and we report the corresponding costs on the bottom rows. With  $u \geq 0$  the feasible fiber is compact and both optima remain close across the sweep; with  $|u_i| \leq \bar{u}_i$  the promptness solution leverages mixed-sign null-space directions, lowering  $\tilde{J}_2$  at the expense of a higher  $\tilde{J}_1$ .

The left column shows the unidirectional case ( $u \geq 0$ ), where the feasible fiber is a compact polygon and both optima remain interior and close across the sweep, yielding a short Pareto arc. The right column shows the bidirectional, box-bounded case ( $|u_i| \leq \bar{u}_i$ ,  $\bar{u}_i = 5$ ), where the promptness solution exploits mixed-sign directions in the allocation null space and saturates actuator bounds as  $\tau_x$  grows, reducing  $\tilde{J}_2$  more aggressively while increasing  $\tilde{J}_1$ . These plots provide a concrete visualization of the fiber-dependent trade-off: cooperative, compact fibers temper the conflict, whereas access to antagonistic directions amplifies it and pushes the promptness optimum to the boundary.

## VI. CONCLUSION

We studied redundancy resolution for multirotors with signed-quadratic actuation through a geometric fiber-bundle formulation, revealing an intrinsic trade-off between *energy* (an  $L_{1.5}$  cost) and *promptness* (a log-determinant manipulability-like barrier on the Gram of the task Jacobian).

Via the diffeomorphism  $u = v|v|$ , the allocation reduces to programs on affine fibers, and the degree of conflict is shown to depend on the fiber geometry and actuator inequalities. A dual-actuator example and a standard hexarotor case demonstrated that unidirectional thrust yields compact feasible fibers with short interior Pareto arcs, whereas bidirectional actuation enables antagonistic co-contraction that drives promptness to hardware bounds—thus explaining when endurance and agility are compatible and when they are fundamentally at odds.

This study opens a new direction for aerial multirotors: principled, geometry-based promptness tuning via Pareto navigation rather than heuristics. Future work will apply the theory to other architectures (e.g., omnidirectional and fully actuated platforms), derive design-agnostic laws valid across configurations, and validate the predicted endurance–promptness envelopes through systematic experiments.

## REFERENCES

- [1] M. Tognon and A. Franchi. “Omnidirectional Aerial Vehicles with Unidirectional Thrusters: Theory, Optimal Design, and Control”. In: *IEEE Robotics and Automation Letters* 3.3 (2018), pp. 2277–2282.
- [2] Dario Brescianini and Raffaello D’Andrea. “Design, Modeling and Control of an Omni-Directional Aerial Vehicle”. In: *Proc. of the IEEE Int. Conf. on Robotics and Automation (ICRA)*. Stockholm, Sweden, 2016, pp. 3261–3266.
- [3] Markus Ryll, Heinrich H. Bülthoff, and Paolo Robuffo Giordano. “A Novel Overactuated Quadrotor UAV: Modeling, Control and Experimental Validation”. In: *IEEE Trans. on Control Systems Technology* 23.2 (2015), pp. 540–556.
- [4] Karen Bodie, Zachary Taylor, Mina Kamel, and Roland Siegwart. “Towards Efficient Full Pose Omnidirectionality with Overactuated MAVs”. In: *Proc. of the 2018 Int. Symposium on Experimental Robotics (ISER)*. Springer, 2020, pp. 85–95.
- [5] Angel Romero, Sihao Sun, Philipp Foehn, and Davide Scaramuzza. “Model Predictive Contouring Control for Time-Optimal Quadrotor Flight”. In: *IEEE Trans. on Robotics* (2022). arXiv:2108.13205.
- [6] Elia Kaufmann, Antonio Loquercio, René Ranftl, Matthias Müller, Vladlen Koltun, and Davide Scaramuzza. “Deep Drone Acrobatics”. In: *Robotics: Science and Systems (RSS)*. 2020.
- [7] Alessandro Saviolo, Guanrui Li, and Giuseppe Loianno. “Physics-Inspired Temporal Learning of Quadrotor Dynamics for Accurate Model Predictive Trajectory Tracking”. In: *IEEE Robotics and Automation Letters* 7.3 (2022), pp. 7809–7816.
- [8] Tsuneo Yoshikawa. “Manipulability of Robotic Mechanisms”. In: *The Int. Journal of Robotics Research* 4.2 (1985), pp. 3–9.
- [9] Federico Califano, Daniël van Dijk, and Wesley Roozing. “A Task-Based Post-Impact Safety Protocol Based on Energy Tanks”. In: *IEEE Robotics and Automation Letters* 7.4 (2022), pp. 8791–8798.
- [10] Vishnu Dev Amara, Jörn Malzahn, Wesley Roozing, and Nikos G. Tsagarakis. “Blending of Series-Parallel Compliant Actuation With Field Weakening Control for Explosive Motion Generation”. In: *IEEE Robotics and Automation Letters* 6.2 (2021), pp. 2076–2083.
- [11] Neville Hogan. “Impedance Control: An Approach to Manipulation”. In: *Proc. of the American Control Conf (ACC)*. 1984, pp. 304–313.
- [12] Etienne Burdet, Rieko Osu, David W. Franklin, Theodore E. Milner, and Mitsuo Kawato. “The Central Nervous System Stabilizes Unstable Dynamics by Learning Optimal Impedance”. In: *Nature* 414.6862 (2001), pp. 446–449.
- [13] David W. Franklin, Rieko Osu, Etienne Burdet, Mitsuo Kawato, and Theodore E. Milner. “Adaptation to Stable and Unstable Dynamics Achieved by Combined Impedance Control and Inverse Dynamics Model”. In: *Journal of Neurophysiology* 90.5 (2003), pp. 3270–3282.
- [14] Paul L. Gribble, Lucy I. Mullin, Nicholas Cothros, and Andrew Mattar. “Role of Cocontraction in Arm Movement Accuracy”. In: *Journal of Neurophysiology* 89.5 (2003), pp. 2396–2405.
- [15] Marc Bodson. “Evaluation of Optimization Methods for Control Allocation”. In: *Journal of Guidance, Control, and Dynamics* 25.4 (2002), pp. 703–711.

- [16] Sangyul Park, Jeongseob Lee, Joonmo Ahn, Myungsin Kim, Jong-beom Her, Gi-Hun Yang, and Dongjun Lee. “ODAR: Aerial Manipulation Platform Enabling Omnidirectional Wrench Generation”. In: *IEEE/ASME Trans. on Mechatronics* 23.4 (2018), pp. 1907–1918.
- [17] *Control Allocation (Mixing) — PX4 Guide*. [https://docs.px4.io/main/en/concept/control\\_allocation](https://docs.px4.io/main/en/concept/control_allocation). Accessed: Feb. 14, 2026. 2026.
- [18] *Adding Custom Attitude Controller to Copter (interaction with mixer)*. <https://ardupilot.org/dev/docs/copter-adding-custom-controller.html>. Accessed: Feb. 14, 2026. 2026.
- [19] Fabio Ruggiero, Vincenzo Lippiello, and Aníbal Ollero. “Aerial Manipulation: A Literature Review”. In: *IEEE Robotics and Automation Letters* 3.3 (2018), pp. 1957–1964.
- [20] Mahmoud Hamandi, Federico Usai, Quentin Sablé, Nicolas Staub, Marco Tognon, and Antonio Franchi. “Design of Multirotor Aerial Vehicles: A Taxonomy Based on Input Allocation”. In: *The Int. Journal of Robotics Research* 40.8-9 (2021), pp. 1015–1044.
- [21] Etor Arza, Welf Rehberg, Philipp Weiss, Mihir Kulkarni, and Kostas Alexis. “Performance-guided Task-specific Optimization for Multirotor Design”. In: *arXiv preprint*. Co-optimization of motor poses with RL/BO/CMA for task performance. 2025.
- [22] Davide Bicego, Jacopo Mazzetto, Ruggero Carli, Marcello Farina, and Antonio Franchi. “Nonlinear Model Predictive Control with Enhanced Actuator Model for Multi-Rotor Aerial Vehicles with Generic Designs”. In: *Journal of Intelligent & Robotic Systems* 100.3–4 (2020), pp. 1213–1247.
- [23] Pierre-Jean Bristeau, Philippe Martin, Erwan Salaün, and Nicolas Petit. “The Role of Propeller Aerodynamics in the Model of a Quadrotor UAV”. In: *European Control Conf (ECC)*. 2009, pp. 3550–3555.
- [24] Stephen Boyd and Lieven Vandenberghe. *Convex Optimization*. Cambridge University Press, 2004.